Phonon transport in Cu$_2$GeSe$_3$: Effects of spin-orbit coupling and higher-order phonon-phonon scattering

Hezhu Shao [1,*] Daquan Ding,[1] Ying Fang,[1] Wei Song,[1] Jielan Huang,[1] Changkun Dong,[1] and Hao Zhang[2,3,†]

[1]*Wenzhou Key Laboratory of Micro-nano Optoelectronic Devices, College of Electrical and Electronic Engineering, Wenzhou University, Wenzhou 325035, China*

[2]*Shanghai Ultra-precision Optical Manufacturing Engineering Center, Department of Optical Science and Engineering, Fudan University, Shanghai 200433, China*

[3]*Yiwu Research Institute of Fudan University, Chengbei Road, Yiwu City, Zhejiang 322000, China*

Much attention has been focused on understanding the mechanism of low lattice thermal conductivity in Cu$_2$GeSe$_3$ diamondlike thermoelectric compounds. For Cu$_2$GeSe$_3$, the underlying origin of low lattice thermal conductivity remains to be clarified. In this work, the first-principles calculations are employed to systematically investigate the effects of spin-orbit coupling, higher-order phonon-phonon scattering, phonon wavelike tunneling, temperature-induced renormalization of phonon and phonon-phonon interaction, and volumetric expanse on the phonon transport of Cu$_2$GeSe$_3$. We show that the spin-orbit coupling results in no detectable change on the phonon frequencies, compared with those obtained without spin-orbit coupling, while it induces slight increase in both Grüneisen parameter and lattice thermal conductivity of Cu$_2$GeSe$_3$, and the underlying mechanism is thoroughly analyzed. With the fourth-order phonon scattering and temperature-induced renormalization, the calculated lattice thermal conductivities are well consistent with the experimental results. Due to the enhanced four-phonon scattering process, there are remarkable reductions for the thermal conductivity. In Cu$_2$GeSe$_3$, the coherences term κ_c contributes increasingly to the total lattice thermal conductivity when temperature arises. And after considering the effects of temperature-induced renormalization and higher-order phonon-phonon interactions, the κ_c would provide $\sim$5% and above 25% of total conductivity at 300 and 800 K, respectively. Our finding clarifies the mechanism of low thermal conductivity in Cu$_2$GeSe$_3$, and benefits the design of similar Cu-based diamondlike materials in thermoelectric applications.

I. INTRODUCTION

Thermoelectric (TE) materials can directly realize energy conversion between heat and electricity, and have been widely applied in power generation and refrigeration [1]. The performance of TE materials could be quantified by the figure of merit, $ZT = S^2\sigma T/\kappa$, where S, κ, σ, and T are the Seebeck coefficient, thermal conductivity, electrical conductivity, and the absolute temperature, respectively. $S^2\sigma$ is the power factor, and thermal conductivity κ consists of both the carriers (κ_e) and lattice (κ_L) contributions. Generally, the complex coupling among these coefficients such as S, κ and σ, hinders the significant improvement of TE performance in materials.

The Cu-based diamondlike chalcogenides have attracted extensive interests in TE application for their good electronic transport and low thermal conductivity [2–15]. Cu$_2$GeSe$_3$ is a typical Cu-based diamond compound. In 2011, Cho et al. prepared Cu$_2$GeSe$_3$ and obtained a low value of lattice thermal conductivity 1.9 Wm^{-1}K^{-1} at room temperature. As concerning the intrinsically heat transport, they ascribed the low thermal conductivity to the high anharmonicity in Cu$_2$GeSe$_3$

[7]. We previously have conducted a study for the lattice dynamics and phonon transport of Cu$_2$GeSe$_3$ by first-principles calculations, and found that the Grüneisen parameter γ, which describes the anharmonicity of a material, of Cu$_2$GeSe$_3$ is only around 1.2 at room temperature [10,12]. It suggests that the anharmonicity in Cu$_2$GeSe$_3$ is normal and much less than that in PbTe ($\gamma \sim 2.0$ by first-principles calculations [40]). Our previous calculations have considered three-phonon scattering processes and got a lattice thermal conductivity of 4.5 Wm^{-1}K^{-1} at room temperature for Cu$_2$GeSe$_3$, which is much larger than the experimental value by Cho et al. Recent experiments by different groups gave the similar low lattice thermal conductivities for Cu$_2$GeSe$_3$ [13–15].

Furthermore, if we fit the temperature-dependent lattice thermal conductivity into a/T^b, the experimental lattice thermal conductivity with respect to temperature by Cho et al. [7], Wang et al. [13], Yang et al. [14], and Hu et al. [15] obeys the $\sim 1/T^{1.28}$, $1/T^{1.12}$, $1/T^{1.40}$, and $1/T^{1.21}$ relations, respectively. We could fit these four groups of experimental results together, and got a relation of $\kappa_L \sim 1/T^{1.26}$. As for the preparation process, Hu et al., Cho et al., and Yang et al. prepared their samples by melting, cooling to ingots, grounding into fine powder followed by hot pressing, and Wang et al. used the spark plasma sintering (SPS) method in the final synthesis step. The relative densities

*hzshao@wzu.edu.cn
†zhangh@fudan.edu.cn

of the first three were 93%, 95%, and 98%, respectively, whereas the relative density of the sample obtained by SPS was 97%. We note that as the density gets closer to 100%, the grain boundary scattering gets lower in materials, and since the grain boundary scattering is independent of temperature [16], the b value would be greater than the value obtained by above experimental results ($\sim$1.26) for intrinsic Cu_2GeSe_3.

According to the theoretical analysis of temperature-dependent lattice thermal conductivity for materials, if only considering three-phonon scattering, the lattice thermal conductivity κ_{3ph} should obey the $\sim 1/T$ relation. The inclusion of higher-order phonon-phonon interaction would increase the degree of declining trend with respect to temperature, i.e., b would be great than 1. Then the experimental results of temperature-dependent lattice thermal conductivity in Cu_2GeSe_3 implied that the higher-order phonon-phonon interaction should be included to describe the behavior of phonon transport. Whereas the mechanism of higher-order phonon-phonon interaction for phonon transport in Cu_2GeSe_3 remains to be revealed.

On the other hand, spin-orbit coupling (SOC) is the key to understanding many fundamental properties of materials, such as topological insulating states [17], Mott metal-insulator transition in strong correlated electron systems [18]. Many topological insulator such as Bi_2Te_3 and SnTe are excellent TE materials. However, the effect of SOC on the phonon transport remains controversial. Tian *et al.* have reported that in PbSe and PbTe, the phonon lifetimes are considerably larger with SOC, which leads to twice larger thermal conductivity with SOC than that without SOC at 300 K [19]. However, Li *et al.* proposed that SOC is not important to the phonon transport of Mg_2Si and Mg_2Sn, considering the relatively small discrepancies between their calculations and the experimental data [20]. Whether SOC has significant influence to the phonon transport properties in Cu_2GeSe_3 remains unclear.

Here we study the effect of SOC and higher-order phonon-phonon scattering together with the effects of wave-like coherent propagation, and temperature-dependent lattice dynamics on the phonon transport for Cu_2GeSe_3. And we compared in detail the phonon dispersion, anharmonicity, and lattice thermal conductivities. Based on the calculations, we also discussed the mechanism of low heat transport in Cu_2GeSe_3.

II. METHODOLOGY

The calculations of structural optimization and total energy were performed by the density functional theory (DFT) method, as implemented in the Vienna *Ab initio* simulation package (VASP) [21,22]. And we employed the generalized gradient approximation with Perdew, Burke, and Ernzerhof functional (PBE) [23]. During optimizing calculations, the plane-wave energy cutoff was set to be 500 eV, the electronic energy convergence was set to be 10^{-5} eV, and the force convergence for ions was 10^{-3} eV/Å. The lattice parameters of Cu_2GeSe_3 were determined by fitting the Birch-Murnaghan third-order equation of state [11].

The phonon spectra and group velocities of phonons were calculated by using Parlinski-Li-Kawazoe method, employing the supercell approach as implemented in the Phonopy package [24,25]. To get the lattice dynamical properties, a $3 \times 3 \times 3$ supercell of primitive cell containing 162 atoms was employed in the calculations of harmonic interatomic force constants, and a Γ-centered $2 \times 2 \times 2$ k-point grid is used to sample the Brillouin zone.

The phonon Boltzmann transport equation method considering both the three-phonon scattering and four-phonon scattering was employed to obtain the phonon lifetime, which was implemented in ShengBTE [26,27]. The lattice thermal conductivity κ_p was calculated by

$$\kappa_p^{xy} = \frac{1}{Nk_BT^2\Omega} \sum_l f_0(\omega_l)(f_0(\omega_l) + 1)(\hbar\omega_l)^2 v_l^x v_l^y \tau_l, \quad (1)$$

where Ω is the volume of unit cell, x and y are the Cartesian components of x, y, or z, k_B is Boltzmann constant, and $f_0(\omega_l)$ is Bose-Einstein distribution function. In addition, the *scale-broad* was set to be 0.1, which is enough to get the convergent phonon transport properties. And during the calculations of lattice thermal conductivity both considering three-phonon scattering and four-phonon scattering, an $8 \times 8 \times 8$ q-point grid was employed to reach convergence.

To obtain the three-phonon and four-phonon scattering the phonon lifetimes, the third-order and fourth-order interatomic force constants (IFCs) should be calculated. In ShengBTE, both the third-order and fourth-order IFCs were obtained by the finite-difference supercell method. For the force calculations, a $3 \times 3 \times 3$ supercells of primitive cell of Cu_2GeSe_3 was employed. And the cutoff for third-order force interaction is 4.7 Å, which was tested to get the convergent Grüneisen parameter γ and lattice thermal conductivities. As for the fourth-order force interaction, we tested the cutoff from second-nearest to sixth-nearest neighboring atoms. There are 788 supercells with different displaced atoms needed to be calculated to get the third-order constants. And for fourth-order force constants calculations, we calculated 1520, 2872, 4520, 7080, and 7928 supercells for second-, third-, fourth-, fifth-, and sixth-nearest neighboring cutoff, respectively, and they corresponds to the cutoff distances of 0.3231, 0.3939, 0.4006, 0.4077, and 0.4320 nm. During the calculations of force, only the Γ point was used for the k-point mesh set.

Due to the strong anharmonicity in Cu_2GeSe_3, we also calculated the off-diagonal coherence phonon lattice thermal conductivity [28]. In the Wigner formalism, the thermal conductivity can be generalized to an expression including the contribution from both the populations and coherences Wigner distribution elements. The former is related to the particlelike propagation of phonon wavepackets and the latter is associated to the wave-like tunneling and loss of coherence between different vibrational modes. The thermal conductivity can be calculated by

$$\kappa_L^{xy} = \kappa_p^{xy} + \kappa_c^{xy}, \quad (2)$$

where

$$\kappa_c^{xy} = \frac{\hbar^2}{Nk_BT^2\Omega} \sum_{l \neq l'} \frac{\omega_l + \omega_{l'}}{2} v_{ll'}^x v_{l'l}^y$$

$$\times \frac{\omega_l f_0(\omega_l)(f_0(\omega_l) + 1) + \omega_{l'} f_0(\omega_{l'})(f_0(\omega_{l'}) + 1)}{4(\omega_l - \omega_{l'})^2 + (1/\tau_l + 1/\tau_{l'})^2}$$

$$\times (1/\tau_l + 1/\tau_{l'}). \tag{3}$$

The key step is to calculate the interband velocity matrix element of $v_{ll'}$

$$v_{ll'}^x = \varepsilon_{l,ba}^* \nabla_{\mathbf{q}}^x \sqrt{D(\mathbf{q})}_{ba,b'a'} \varepsilon_{l',b'a'}, \tag{4}$$

where ε and ε^* are the eigenvector component and the corresponding conjugate, $D(\mathbf{q})$ is the dynamical matrix. We use a home-made *Mathematica* program (KcMath) to calculate the κ_c^{xy}.

In the KcMath, we use the difference method to calculate the $\nabla_{\mathbf{q}}^x \sqrt{D(\mathbf{q})}_{ba,b'a'}$, the employed difference formula is $f'(x) = (f(x + h) - f(x - h))/(2h)$ with the error of h^2. Then $\nabla_{\mathbf{q}}^x \sqrt{D(\mathbf{q})}_{ba,b'a'}$ can be approximated with $(\sqrt{D(\mathbf{q} + dq_x)} - \sqrt{D(\mathbf{q} - dq_x)})/(2dq_x)$, where we set $dq_x = 0.01\text{Å}^{-1}$. We use the inner function of MatrixPower of *Mathematica* to calculate the $\sqrt{D(\mathbf{q} \pm dq_x)}$. For the q points, we use the q-mesh set of BTE.qpoints_full in ShengBTE. Then we employed Phonopy to construct the dynamical matrix at these q points and the $q \pm dq_x$ points. After obtaining the $v_{ll'}^x$, together with the ω_l, $1/\tau_l$ by ShengBTE, we could use the formula of (3) to calculate the κ_c^{xy} (see Supplemental Material [29]).

To study the different temperature-induced effects on the lattice thermal conductivity, we employed the stochastically initialized temperature-dependent effective potential method [30,31] (s-TDEP) together with VASP to extract the harmonic and anharmonic, including third and fourth IFCs, then fed these IFCs in ShengBTE to calculate the phonon-phonon scattering. A conventional TDEP calculation includes thermostatting a supercell, and then obtaining the forces and displacements with respect to time. These forces and displacements are calculated by first-principles packages. We take these sets of forces and displacements to fit the coefficients in an effective lattice dynamical Hamiltonian. Then the second, third, and fourth IFCs are obtained by a least-squares algorithm from these force-displacement datasets.

Here we employed an efficient stochastic sampling method to conduct a simulation cell in uncorrelated thermally excited states [31]. The first step is to obtain a set of force constants defined by a Debye temperature, which is from previous calculations [11]. Such force constants can be used to seed the calculations to generate a set of displacements. The second step is to perform a series of first-principles calculations for the obtained snapshots to get a set of force-displacement datasets, which are used to obtain IFCs. Then with the IFCs, one can generate a new snapshots, and repeat the procedure until self-consistency. We used 50 configurations during each round to obtain the IFCs, and the results were typically converged within four iterations.

To determined the temperature-dependent volume, we perform calculations on a temperature-volume grid including six temperature and seven volumes. We select the six temperature

as $T = \{300, 400, 500, 600, 700, 800\}$ K and the seven volumes linearly spaced within 1.00 to 1.06 times of 0 K equilibrium volume. Then we minimize the Helmholtz free energy $F(T, V)$ by fitting the Birch-Murnaghan third-order equation of state [11] to obtain the equilibrium volume at each temperature.

III. RESULTS AND DISCUSSION

A. Atomic structure, phonon dispersion, and the LO-TO splitting correction

As shown in Fig. 1(a), Cu₂GeSe₃ has orthorhombic structure with space group of *Imm*2 [32]. The basic vectors of primitive cell of Cu₂GeSe₃ can be written as $\frac{1}{2}(-a, b, c)$, $\frac{1}{2}(a, -b, c)$, and $\frac{1}{2}(a, b, -c)$, and the corresponding first Brillouin zone is given in Fig. 1(b). The unit cell of Cu₂GeSe₃ contains six atoms, among them there are two types of Se sites. Se₁ site on $2a$ $(0, 0, 0)$ is bonded by two germanium and two copper atoms, and Se₂ site on $4c$ $(x, 0, 0)$ ties with one germanium and three copper atoms. We determined the lattice parameters of Cu₂GeSe₃ by fitting the Birch-Murnaghan third-order equation of state [11]. The relaxed parameters of a, b, and c by PBE method are 5.943 Å, 2.029 Å, and 2.796 Å, respectively, which are slightly larger than the experimental values of 5.927 Å, 1.977 Å, 2.744 Å [33]. The structural parameters and atomic positions are given in the Supplemental Material [29]. To study the effect of SOC on the structure, we also compared the equilibrium volumes by the calculations with SOC and without SOC. As shown in Fig. 1(c), SOC leads to a very slightly change (with ignorable 0.05% in relatively volumetric increase) to the optimized volume for Cu₂GeSe₃. To obtain the phonon spectra, we should firstly calculate the harmonic force constants. Generally, both the resultant accuracy and efficiency would be affected by the cutoff energies (E_C) for plane wave basis and k-sampling set in the calculations. The calculated phonon spectra of Cu₂GeSe₃ are given in Fig. 1(d). For comparison, the experimental data of Raman scattering [33] are also plotted. From Fig. 1(d), we can see that the calculation of harmonic force constants with $E_C = 295.4$ eV gives well convergent phonon frequencies for Cu₂GeSe₃. Considering a large amount of supercells with large number of atoms are needed to be employed in the calculations to obtain phonon transport property, we used the value of 295.4 eV for E_C to calculate the anharmonic force constants.

In our previous calculations, we used a supercell containing 72 atoms to obtain the harmonic force constants [10]. To obtain a more reliable phonon spectra, here we employed a larger supercell, which contains 162 atoms, to calculate the phonon spectra and plotted it in Fig. 1(d). We also list the calculated Raman frequencies and their symmetries in Table I. Mostly, two situations give convergent phonon dispersion of Cu₂GeSe₃, while there are some very slight difference in frequencies. For example, for a Raman mode with the frequency of 135 cm⁻¹ as demonstrated in experiment [33], previous calculation gave an A_1 mode with 138.2 cm⁻¹ and a B_1 mode with 136.4 cm⁻¹, while the current calculation presents 136.7 cm⁻¹ and 136.0 cm⁻¹ for these A_1 and B_1 mode, respectively. On the other hand, the calculated Raman frequencies by us-
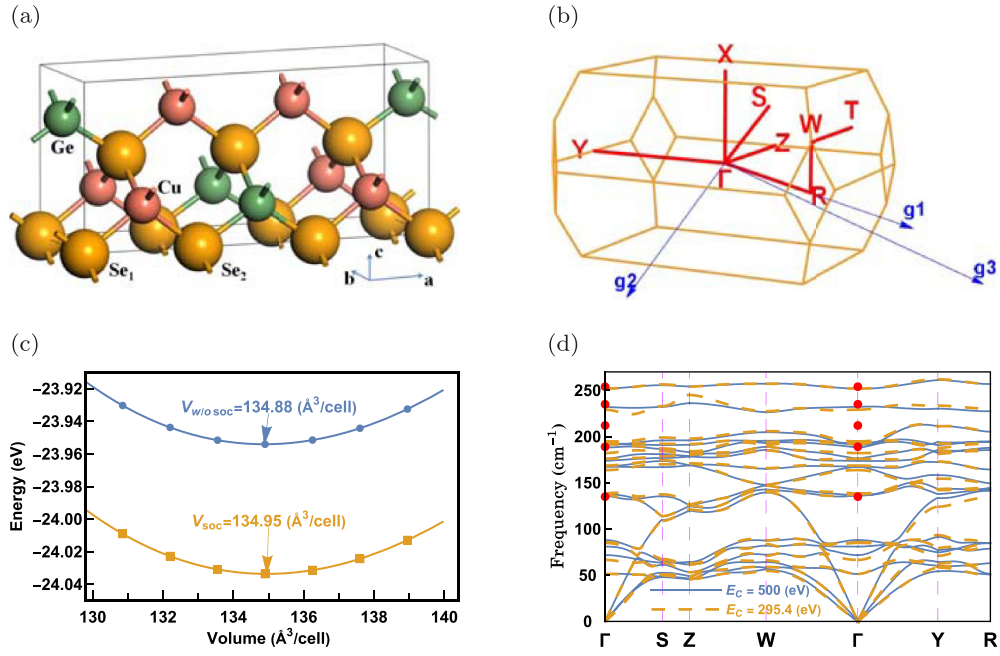
FIG. 1. The structure and phonon spectra of Cu_2GeSe_3. (a) Crystal structure, (b) Brillouin zone, where $\Gamma = (000)$; $T = (\frac{1}{2}\frac{\bar{1}}{2}0)$; $W = (\frac{3}{4}\frac{\bar{1}}{4}\frac{\bar{1}}{4})$; $R = (\frac{1}{2}00)$; $S = (\frac{1}{2}0\frac{\bar{1}}{2})$; $X = (\frac{1}{2}\frac{\bar{1}}{2}\frac{\bar{1}}{2})$, (c) the structural optimization curves by PBE method with and without SOC, and (d) phonon spectra, where the blue line is for cut-off energy of 500 eV and orange dashed line for cut-off energy of 295.4 eV, the red solid circles are the Raman data from Ref. [33].

ing a smaller supercell in previous calculations are in good agreement with the experimental data, except for a B_2 (around 212 cm^{-1}). For the B_2 mode, the calculated frequency is 21 cm^{-1} lower than the experimental value [10]. Here, using a larger supercell is unable to meliorate the prediction of calculation. As listed in Table I, the difference between the calculated and experimental frequency for the B_2 mode is still around 21 cm^{-1}.

In previous work, we speculated that the difference between the calculational and experimental results for B_2 mode may be from the LO-TO splitting [10]. DFT calculations predict a metallic ground state for Cu_2GeSe_3 (see the Supplemental Material [29]), which are consistent with the results in Material Projects [34]. SOC cannot open the band gap for Cu_2GeSe_3. The present calculations cannot reproduce the experimental band gap of around 0.8 eV for Cu_2GeSe_3 [35,36]. Recently, Hu *et al.* have reported a calculated band structure with a band gap of about 0.07 eV for Cu_2GeSe_3. Hu *et al.* employed a supercell containing 24 Cu_2GeSe_3 unit to

calculate the band structure, while we could not reproduce the semiconductor behavior by using such supercell structure (see Supplemental Material [29]). It is hard to get a convergent dielectric constant by standard DFT calculation, thus the LO-TO splitting could not be considered in previous calculations [10]. Here, to give a reasonable estimation for the LO-TO splitting in Cu_2GeSe_3, we combine the experimental frequency of B_2 mode, calculated dielectric constant, and the Born effective charge of similar Cu-based diamondlike chalcogenide of Cu_2GeS_3 and BiCuOSe [37], a layer compound containing Cu-Se network with similar chemical bonds with Cu_2GeSe_3. In the calculations, LO-TO splitting is introduced by adding a nonanalytical correction to the dynamical matrix [38,39]

$$\tilde{D}_{\tau\alpha}^{\tau'\alpha'}(\mathbf{q}) = D_{\tau\alpha}^{\tau'\alpha'}(\mathbf{q}) + \frac{4\pi}{\sqrt{M_\tau M_{\tau'}}\Omega_0} \frac{(\mathbf{q} \cdot \mathbf{Z}_{\tau\alpha})(\mathbf{q} \cdot \mathbf{Z}_{\tau'\alpha'})}{\mathbf{q}^T \varepsilon \mathbf{q}} e^{-\frac{q^2}{\rho^2}},$$

(5)

TABLE I. Theoretically determined Raman frequencies (in cm^{-1}) and their symmetry assignments of the experimental results [33].

Raman scattering		Cal. w/o LO-TO [10]		Cal. w/o LO-TO	Cal. with LO-TO
Symmetry	Frequency	Symmetry	Frequency	Frequency	Frequency
A_1 or B_1	135	B_1	136.4	136.0	136.0
		A_1	138.2	136.7	136.7
A_2	189	A_2	193.0	192.8	192.8
B_2	212	B_2	191.4	191.3	211.9
A_1 or B_1	235	A_1	235.5	232.4	232.4
A_1 or B_1	254	B_1	252.2	252.3	252.3
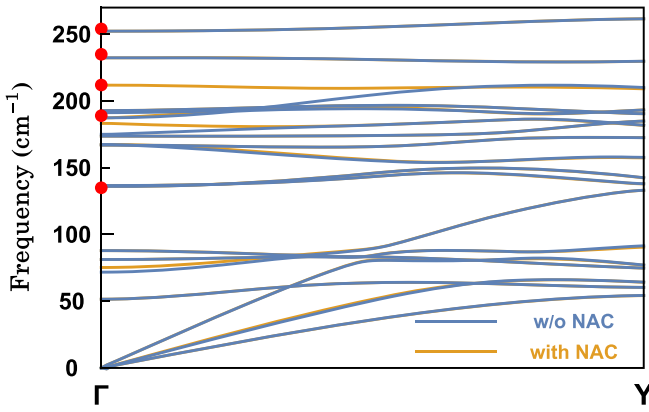
FIG. 2. The phonon spectra along Γ–Y obtained from the dynamical matrix with nonanalytical correction.

where **Z**, ε, and Ω_0 are the Born effective charge, dielectric constant, and primitive cell volume, respectively. Also, the dynamical matrix of the crystal

$$D_{\tau\alpha}^{\tau'\alpha'}(\mathbf{q}) = \sum_n \frac{1}{\sqrt{M_\tau M_{\tau'}}} \Phi_{\tau\alpha}^{\tau'\alpha'}(n) \exp(i\mathbf{q}\cdot\mathbf{R}_n), \quad (6)$$

where n denotes the nth primitive cell in supercell and $\mathbf{R}_n$ a translation vector for the nth primitive cell, τ and M_τ refer to the atom and its mass in the primitive cell, α is the Cartesian components of x, y, or z, and $\Phi_{\tau\alpha}^{\tau'\alpha'}$ is the harmonic force constants. From the above expression, the nonanalytical term describing the LO-TO splitting effect is direction dependent. For the B_2 mode, all atoms vibrate along the y direction, then the main correction due to LO-TO splitting comes from the direction of Γ–Y. Thus we should estimate the matrix elements of yy of dielectric constant (ε^{yy}) and Born effective charge ($\mathbf{Z}_{Cu}^{yy}$, $\mathbf{Z}_{Ge}^{yy}$, and $\mathbf{Z}_{Se}^{yy}$). The calculated ε^{yy} of Cu$_2$GeS$_3$ is 20.18. In Cu$_2$GeS$_3$, the yy elements of Born effective charge of Cu$_1$, Cu$_2$, Ge, S$_1$ (bonds to two Ge and two Cu atoms), S$_2$ (bonds to one Ge and three Cu atoms), and S$_3$ (bonds to one Ge and three Cu atoms) are 1.0, 1.0, 2.9, -2.0, -1.7, and -1.2, respectively. In usual chalcogenide, the Born effective charge increases from sulfide, to selenide, to telluride, such as in PbCh (Ch=S, Se, and Te) [40]. In BiCuOSe, the calculated ε^{yy} is 18.64, and the yy elements of Born effective charge of Cu and Se are around 1.5 and -3.7, respectively [37,41]. Then we deliberately took the values of $\varepsilon^{yy} = 20$, $\mathbf{Z}_{Cu}^{yy} = 1.5$, $\mathbf{Z}_{Ge}^{yy} = 4.5$, $\mathbf{Z}_{Se_1}^{yy} = -3$, and $\mathbf{Z}_{Se_2}^{yy} = -2.25$ as the input of nonanalytical correction to the dynamical matrix for Cu$_2$GeSe$_3$. As listed in Table I, the B_2 mode is corrected to 211.9 cm^{-1}. And we plot the phonon dispersion with LO-TO splitting along Γ–Y in Fig. 2, in which the calculated Raman frequencies are in excellent agreement with the experimental data.

We note here that the good agreement between the theoretical calculations and the experimental results shows the suitability of the calculation method. In addition, we should also see that in the current DFT calculation, the results of 0 K equilibrium volume are considered, but the experiments were conducted at room temperature. The theoretical failure to consider the effect of temperature and volume change exactly compensates for the error caused by the overestimation of the

PBE for the volume. In the following paragraphs, we will study the temperature-induced effects and thermal expansion on phonon frequency and phonon transport.

B. The effect of SOC on the phonon transport

Now we study the effects of SOC on the phonon dispersion and thermal conductivity. We calculated the harmonic force constants with and without SOC for Cu$_2$GeSe$_3$, and obtained the phonon spectra, as shown in Fig. 3(a). Though SOC brings splitting for the valence bands, and lower the total energies by around 2 eV for each supercell of Cu$_2$GeSe$_3$, it results in no detectable change on the phonon frequencies, compared with those obtained without SOC.

Next we investigate further the effect of SOC on phonon transport of Cu$_2$GeSe$_3$. Figure 3(b) shows that SOC has very little impact on the mode Grüneisen parameters. The averaged mode Grüneisen parameter as shown in Fig. 3(c) indicates that the certain temperature is 39 K, i.e., the expansion coefficient will change from negative to positive at this point as the temperature changes. This is consistent with our previous calculations by quasiharmonic approximation [10]. The SOC brings some increase in the averaged Grüneisen parameters. The difference between that with SOC and without SOC becomes less and less with temperature goes higher, though remains more than 0.01. Figure 3(d) shows that SOC also enhance the lattice thermal conductivity. The relative difference of κ_L with and without SOC, $\Delta\kappa_R = (\kappa_{\text{with}} - \kappa_{w/o})/\kappa_{w/o}$, decrease from 5.27% at 200 K to 5.20% at 800 K.

SOC induces a slight increase in both Grüneisen parameter and lattice thermal conductivity of Cu$_2$GeSe$_3$. This is not common for usual materials, since the increasing in Grüneisen parameter means enhancing the anharmonicity, and thus the phonon scattering will be strengthened accordingly and the lattice thermal conductivity would decrease. Nevertheless, in Cu$_2$GeSe$_3$, low-frequency (under 88 cm^{-1}) phonons including most acoustic and several optical modes exhibit negative mode Grüneisen parameter, as shown in Fig. 3(b), and these modes will increase with expansion of volume. Accordingly, Cu$_2$GeSe$_3$ shows negative expansion at low temperatures, since the low-frequency modes of Cu$_2$GeSe$_3$ are mainly active. Thus, the increase induced by SOC in the values of Grüneisen parameters of low-frequency modes means that the scattering rate of these phonons in Cu$_2$GeSe$_3$ is weakened. Furthermore, due to the low-frequency phonon modes determining the lattice thermal conductivity in Cu$_2$GeSe$_3$ [12], SOC enhances slightly the lattice thermal conductivity of Cu$_2$GeSe$_3$.

C. Higher order phonon-phonon scattering and the wavelike interbranch tunneling

In Cu$_2$GeSe$_3$, the isotopic scattering is negligible compared to the three-phonon scattering [12], then the phonon transport of intrinsic Cu$_2$GeSe$_3$ is determined mainly by the effect of anharmonic phonon-phonon scattering including three-phonon and four-phonon scattering. Figure 4(a) gives the temperature-dependent lattice thermal conductivity of Cu$_2$GeSe$_3$. The thermal conductivity calculation considering only three-phonon scattering greatly overestimates the
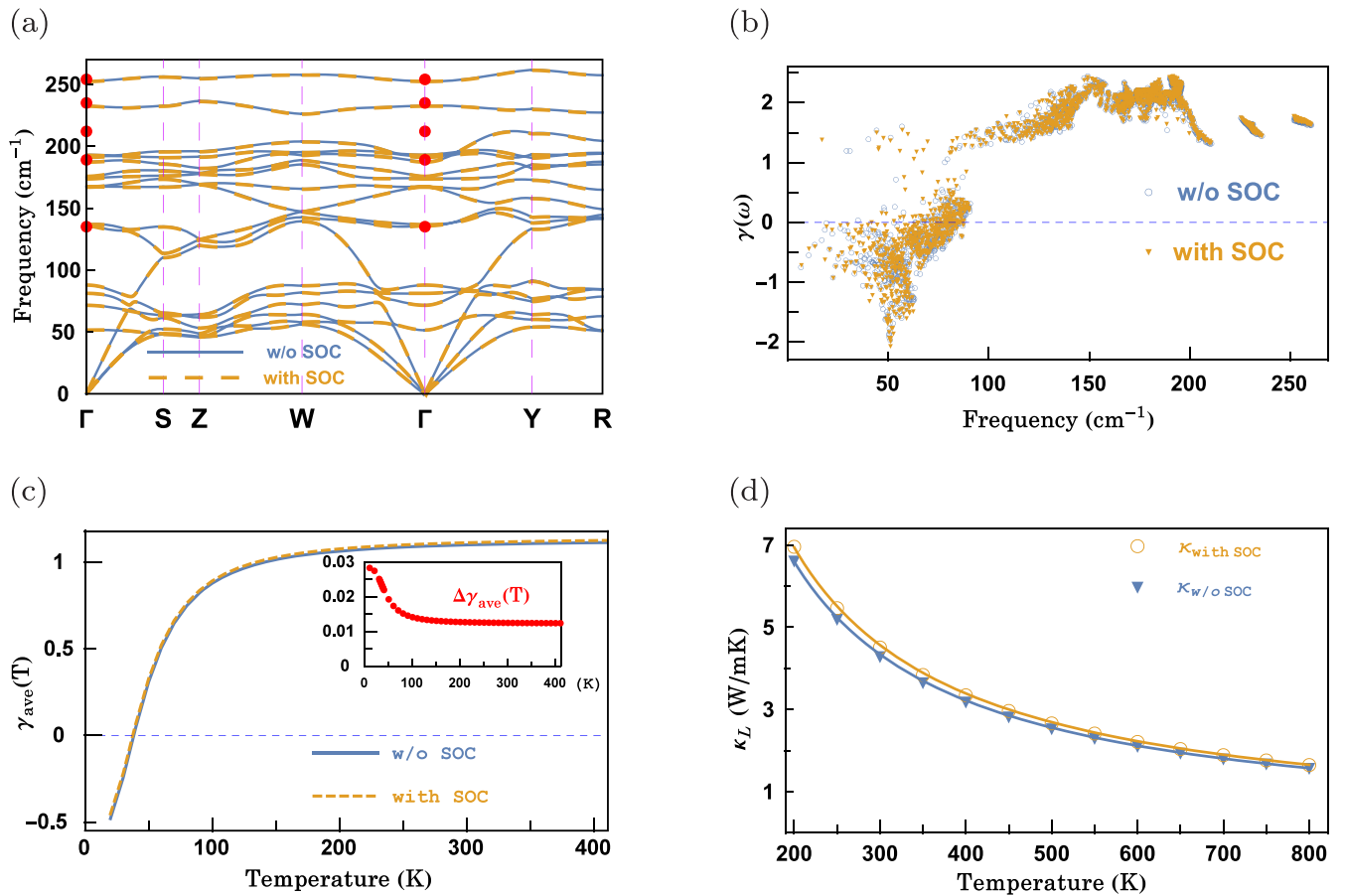
FIG. 3. The effect of SOC on the phonon transport of Cu$_2$GeSe$_3$. Phonon spectra (a), the blue line is for without SOC and dashed orange line for with SOC, frequency-dependent mode Grüneisen parameter (b), averaged Grüneisen parameter (c) and lattice thermal conductivity (d) with respect to temperature.

thermal conductivity, compared with the experimental values [7,13–15]. When we adopted only second nearest neighbors as the cutoff, which is a common strategy in other works [27,42,43], for the fourth-order force interactions, with the addition of four-phonon scattering to the three-phonon scattering, we obtained values of lattice thermal conductivity that are in good agreement with the experimental values. At 300 and 500 K, four-phonon scattering leads to reduction to the lattice thermal conductivity by 53% and 63%, respectively. When the temperature arises to 800 K, the reduction reaches to 72%.

We tested different cutoff for the fourth-order force interaction and found it would cost too much to calculate the convergent lattice thermal conductivity. In the following, we will discuss the results by considering fourth nearest neighbors for the fourth-order force interactions. The calculations show that when the fourth-order phonon scattering is considered, the lattice thermal conductivity will drop sharply. At 300 and 500 K, four-phonon scattering results into the reduction for the lattice thermal conductivity by 82% and 87%, respectively. Figure 5(a) shows the phonon lifetimes of Cu$_2$GeSe$_3$ at 300 K. Four-phonon scattering results in much lower phonon lifetimes (by ∼ one order of magnitude) than that by three-phonon scattering, especially in the range of under 80 cm^{-1}. For the modes with higher frequencies than 80 cm^{-1},

the lifetime due to four-phonon scattering is much higher than that by three-phonon scattering. According to Mattiessen's rule [44], $1/\tau_T = 1/\tau_{3ph} + 1/\tau_{4ph}$. The four-phonon scattering would bring remarkable influence to the low frequency modes and then the lattice thermal conductivity. In Cu$_2$GeSe$_3$, the phonon modes with frequencies lower than 88 cm^{-1} contribute mostly to the lattice thermal conductivity [12]. Then even at a low temperature of 300 K, the four-phonon scattering will lead to a dramatic reduction for lattice thermal conductivity.

To quantitatively evaluate the effect of four-phonon scattering on phonon transport of Cu$_2$GeSe$_3$, we give the phonon lifetime (τ_{3ph}) due to three-phonon scattering and the total phonon lifetime (τ_T) considering both the three-phonon and four-phonon scattering at 300 and 500 K in Fig. 5(b). We fit the frequency-dependent lifetimes with the equation of c/ω^2. At 300 K, $c_{3ph} = 36275.3$ and $c_T = 4021.8$, which means that the phonon lifetime drops by about 89% due to four-phonon scattering. At 500 K, $c_{3ph} = 21363.3$ and $c_T = 1541.5$, which implies that the four-phonon scattering reduces the phonon lifetime by 93%. The increase in the four-phonon scattering effect with increasing temperature is common in other materials such as C, Si, BAs etc. [27,42].

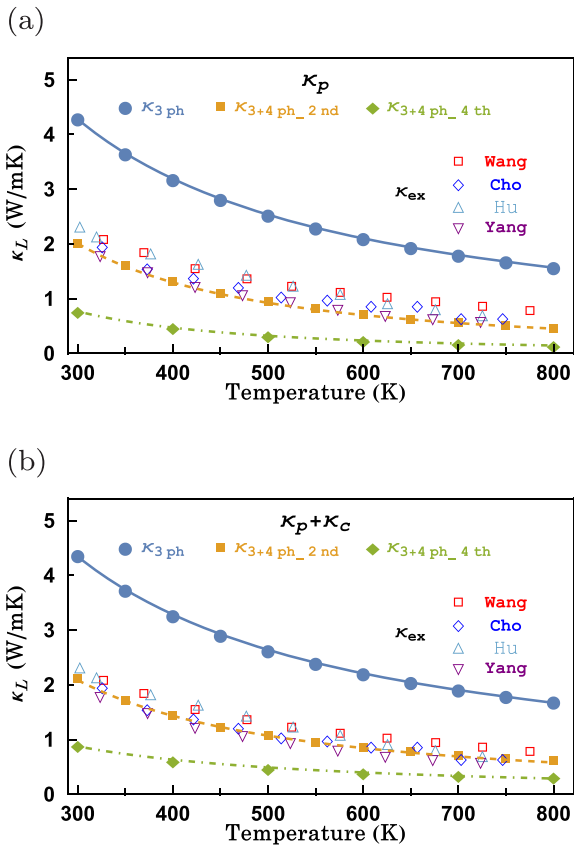We now analyze the reasons why the four-phonon effect is so strong in Cu$_2$GeSe$_3$. Following the argument of Feng

FIG. 4. Average lattice thermal conductivities with respect to temperature, (a) for κ_p, and (b) for $\kappa_p + \kappa_c$, the experimental values by different groups [7,13–15] are given for comparison.

et al. [42], we also employed $r_{43} = |\Phi 4_{max}/\Phi 3_{max}|^2/|\Phi 2_{max}|$ to semiquantitatively estimate the importance of fourth order to the third-order anharmonicity for Cu$_2$GeSe$_3$. Figures 6(a) and 6(b) give the third-order IFCs and fourth-order IFCs with respect to the largest length of the side of triangle and quadrilateral, respectively. In Cu$_2$GeSe$_3$, $r_{43} = 1.74$, which is much larger than that in Si (0.16), BAs (0.12), and Diamond (0.13). On the other hand, there is remarkable fourth-order anharmonicity in BAs due to large four-phonon scattering phase space. We used the phase space ratio of $p_{43} = |p4/p3|$ as second index to estimate the importance of fourth-order importance. In BAs, $p_{43} = 10.44$, while here in Cu$_2$GeSe$_3$, p_{43} is merely 0.85. Then the strong fourth order anharmonicity should ascribed to the larger anharmonicity ratio of r_{43}.

We look further into the contributions of different processes to the four-phonon scattering. As shown in Fig. 7(a), the dominant scattering channels for the acoustic modes in Cu$_2$GeSe$_3$ are the recombination processes $q3 = q + q1 - q2 + Q$ and the absorption processes $q3 = q + q1 + q2 + Q$, where Q is a reciprocal lattice vector. As $Q = 0$ is for normal processes and nonzero for Umklapp processes. The dominant scattering channels for optical branches are the recombination processes $q3 = q + q1 - q2 + Q$ and the splitting processes $q3 = q + q1 + q2 + Q$. For all these scattering processes, the recombination processes makes the main

contributions to the four-phonon scattering in Cu$_2$GeSe$_3$. As shown in Fig. 7(b), in Cu$_2$GeSe$_3$, the Umklapp processes is dominant.

From the above discussion, we see that the calculated value of thermal conductivity is much lower than the experimental values after considering the fourth-order phonon scattering. There is a strong anharmonicity in Cu$_2$GeSe$_3$, so that the phonon linewidths are much larger than the interbranch spacings, especially at high temperatures as shown in Fig. 8, where in the spectra function we only consider three-phonon scattering. Is it possible that considering the wavelike transport behavior of phonons [28] will compensate for the overestimation of higher order phonon-phonon scattering? We adopt a/T^b equation to fit the behavior of temperature-dependent lattice thermal conductivity for κ_{p-3ph}, $\kappa_{p-3ph} + \kappa_{c-3ph}$, $\kappa_{p-3ph+4ph}$, and $\kappa_{p-3ph+4ph} + \kappa_{c-3ph+4ph}$ to estimate the effects of the wavelike interbranch tunneling to lattice thermal conductivity. For the lattice thermal conductivity due to only three-phonon scattering, the $b = 1.025$. When considering the wavelike interbranch tunneling, the $b = 1.008$. For the lattice thermal conductivity due to three-phonon and four-phonon scattering, the $b = 1.705$. When considering the effect of wavelike interbranch tunneling, the $b = 1.135$. The interbranch thermal conductivities increase with respect to the temperature. Quantitatively, when only third-order phonon scattering is considered, the phonon thermal conductivity contribution by the wavelike interbranch tunneling as a percentage of the total ranges from 1.7% at 300 K to 6.9% at 800 K. While considering both the three-phonon and four-phonon scattering, the phonon thermal conductivity contributed by the wavelike interbranch tunneling as a percentage of the total lattice thermal conductivity ranges from 13.9% at 300 K to 54.6% at 800 K. As shown in Fig. 4(b), although wavelike interbranch tunneling contributes rather to the total lattice thermal conductivity, the calculated results including the four-phonon scattering are still much lower than the experimental values for the range of 300 to 800 K.

D. Temperature-induced renormalization for phonon and phonon-phonon interaction at a constant volume

In the above subsection, we just employed DFT calculations for Cu$_2$GeSe$_3$ to study the phonon, three-phonon and four-phonon interaction by calculate the atomic force constants at a constant volume at 0 K. Cu$_2$GeSe$_3$ showed very strong anharmonicity, especially for the fourth-order interaction in phonon-phonon scattering. For the materials with strong anharmonicity, the lattice thermal transport would be affected greatly by temperature [45,46], because the phonon and phonon-phonon interaction are all temperature dependent. Xia showed that anharmonic phonon renormalization could lead to rather vibrational frequency shifts in PbTe and result into a decrease for the phonon-phonon scattering [45]. Errea *et al.* developed the stochastic self-consistent harmonic approximation theory [47–49] to treat the anharmonicity renormalization to the phonon, and successfully applied the method to many strongly anharmonic materials. Tadano *et al.* employed the self-consistent phonon theory to calculate the anharmonic phonon frequency and phonon lifetime in several severely anharmonic systems [50]. In above discussion, we
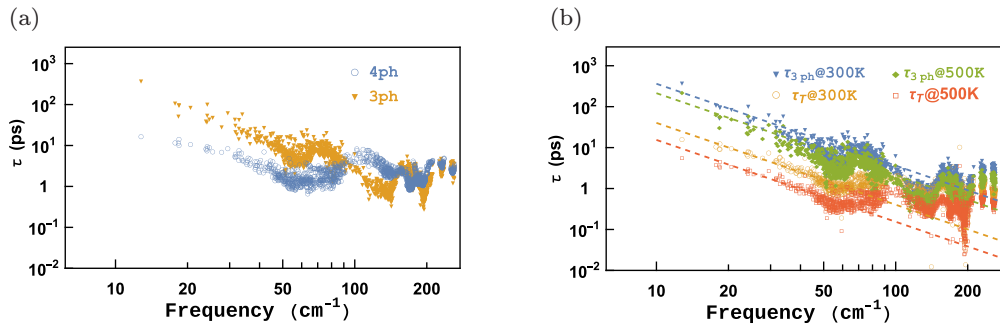
FIG. 5. Phonon lifetimes of Cu_2GeSe_3. (a) Frequency-dependent phonon lifetimes due to three-phonon and four-phonon scattering at 300 K, (b) Frequency-dependent phonon lifetimes at 300 and 500 K.
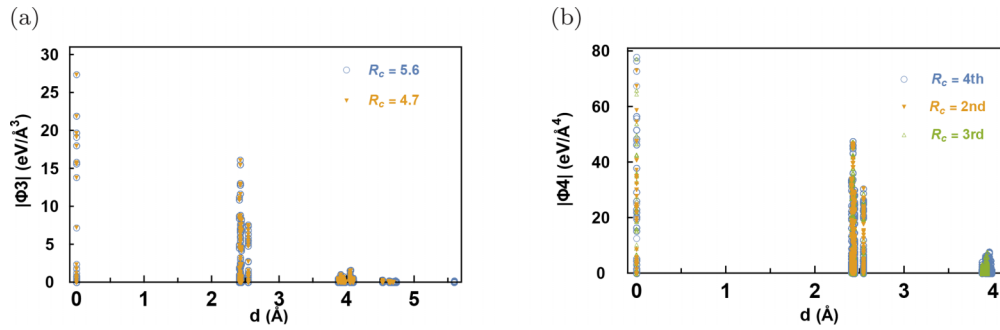

FIG. 6. The interatomic force constants with respect to largest length of the side of triangle (a) for third-order FCs and quadrilateral (b) for fourth-order FCs.
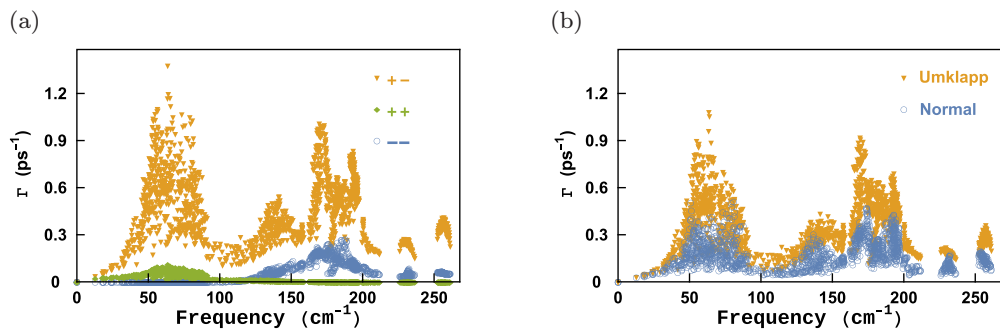

FIG. 7. (a) The contribution to τ_{4ph}^{-1} from allowed scattering channels with respect to frequency, and (b) the Umklapp and normal processes of four-phonon scattering at 300 K for Cu_2GeSe_3.
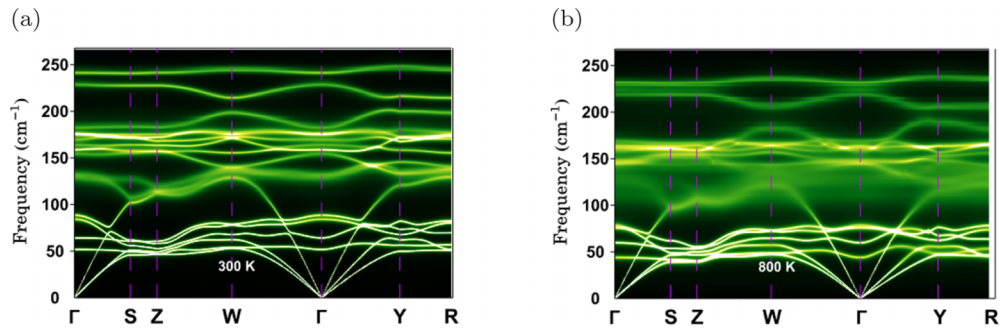
FIG. 8. Phonon spectral function along the high-symmetry directions for Cu_2GeSe_3 (a) at 300 K and (b) at 800 K.
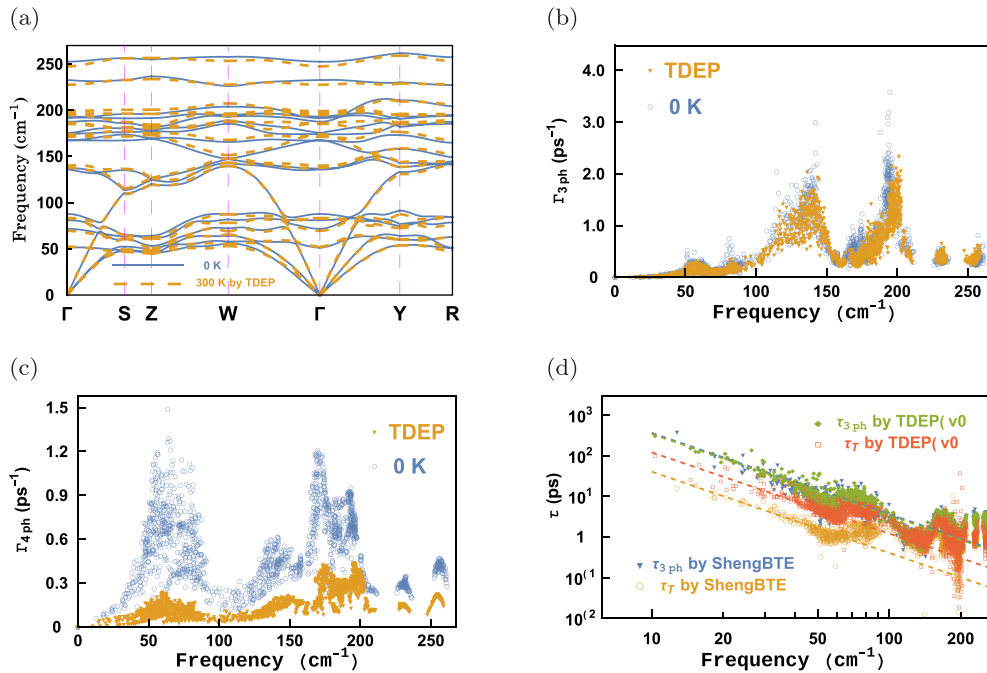
FIG. 9. The effect of temperature-induced renormalization for phonon and phonon-phonon interaction. (a) Phonon spectra, (b) three-phonon scattering rate at 300 K, (c) four-phonon scattering rate at 300 K, and (d) phonon lifetimes of Cu$_2$GeSe$_3$ at 300 K.

have not include the four-order anharmonicity renormalization to the phonon. This is probably a reason for the severe underestimation for the lattice thermal conductivity as compared to the experimental results.

Next we employ TDEP method [30] to study the temperature-induced renormalization for phonon and phonon-phonon interaction at constant volume for Cu$_2$GeSe$_3$. Compared with the calculations at 0 K, TDEP gives a larger harmonic force constants for Cu atom with 4.86 eV/Å^2 for Cu-Cu$_{xx}$ (4.64 eV/Å^2 at 0 K), and for Ge atom with 6.83 eV/Å^2 for Ge-Ge$_{zz}$ (6.65 eV/Å^2 at 0 K), while a slightly smaller value of 5.30 eV/Å^2 for Ge-Ge$_{yy}$ (5.46 eV/Å^2 at 0 K). As depicted in our previous work [10], the Cu atoms contributed mainly to the frequencies between 40 ∼ 80, 125 ∼ 155, and 175 ∼ 200 cm^{-1}, the Ge atoms contributed mainly to the high-frequency modes above 220 cm^{-1}. Figure 9(a) shows the calculated phonon dispersion of Cu$_2$GeSe$_3$ by TDEP method at 300 K. It reflects the comparison of the harmonic force constants, i.e., the higher (lower) values of harmonic force constants leads to higher (lower) frequencies. Figure 9(b) gives the three-phonon scattering rates by different method at 300 K, which shows that the TDEP gives similar strength for the three-phonon scattering rates, with a slight decrease in phonon lifetimes due to three-phonon scattering by 6.7% for c_{3ph} (33843.0), as compared with that from calculated third-order force constants by 0 K. Totally, the temperature-induced renormalizations for phonon dispersion and three-phonon interaction are insignificant.

Figure 9(c) shows that the four-phonon scattering rates at 300 K for Cu$_2$GeSe$_3$ by TDEP are remarkably lower than that from the calculated fourth-order force constants by 0 K. This implies that the temperature-induced renormalization for the four-phonon interaction are significant, especially for the low

frequencies modes lower than 100 cm^{-1}. Such effect results into a substantial increase in the total phonon lifetimes as shown in Fig. 9(d). The c_T by TDEP method is ∼3 times (12084.0) as that from the calculations with the second-, third-, and fourth-order force constants at 0 K. At 300 K, when considering the effects of temperature-induced renormalization for the phonon and phonon-phonon interaction, due to four-phonon scattering, the phonon lifetime drops by 64%.

We used the second-, third-, and fourth-order force constants at 300 K by the TDEP method to calculate the temperature-dependent lattice thermal conductivities as shown in Fig. 10. After considering the effects of four-phonon interaction and the temperature-induced renormalizations for phonon and especially the four-phonon scattering, the calculations give a well consistent lattice thermal conductivities
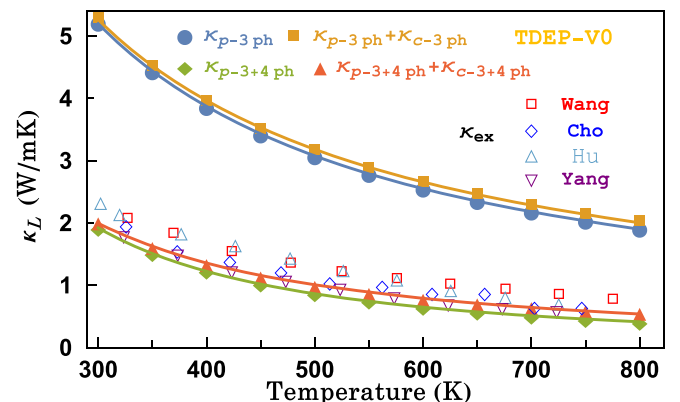

FIG. 10. Average lattice thermal conductivities with respect to temperature in Cu$_2$GeSe$_3$ by TDEP method.
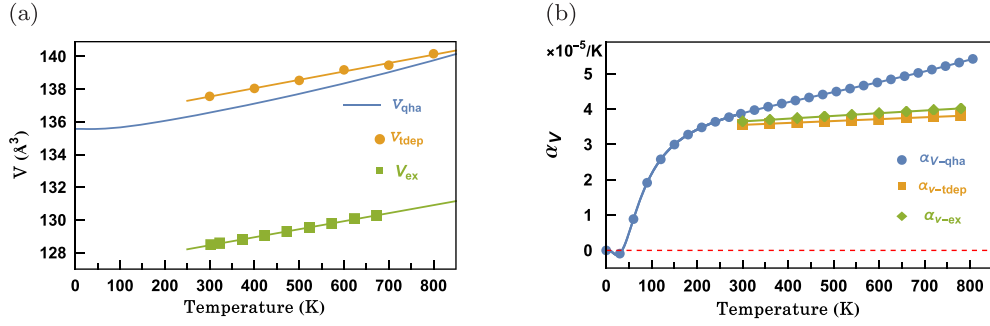
FIG. 11. Calculated temperature-dependent volume (a) and expansion (b) by quasiharmonic approximation and TDEP method for Cu_2GeSe_3 compared with experimental measurements [51].

with the experimental results. Fitting for the lattice thermal conductivity due to three-phonon and four-phonon scattering (merely three-phonon interaction), we get the $b = 1.568$ (1.028). When considering the effect of wavelike interbranch tunneling, the $b = 1.336$ (0.986).

E. Volumetric expansion

In the above discussion, we have not involved the influence of volumetric expansion to the lattice thermal conductivity. Now we study further the effects of volumetric expansion on the phonon transport in Cu_2GeSe_3. Figure 11 shows the calculated volume and volumetric expansion with respect to the temperature. By using the PBE functional, both the quasiharmonic approximation (QHA) and TDEP method overestimate the volume for Cu_2GeSe_3 Fig. 11(a)]. As shown in Fig. 11(b), the QHA overestimates the volumetric expansion as well, while TDEP method gives a well consistent behavior for the volumetric expansion of Cu_2GeSe_3.

Figure 12 shows the effects of volumetric expansion on the phonon transport of Cu_2GeSe_3. With the increase of temperature, the volume will expand, and the phonon dispersion will be red-shifted [see Fig. 12(a)], and the three- and four-phonon interaction will be strengthened [Fig. 12(b)], then the phonon lifetimes will drop after considering the expansion of volume in Cu_2GeSe_3 as shown in Fig. 12(c). We note here that the four-phonon scattering is similar to the three-phonon scattering under 80 cm^{-1}, Because the phonon modes under 80 cm^{-1} contribute mostly to the lattice thermal conductivity, then four-phonon scattering still brings forth significant influence to the phonon transport in Cu_2GeSe_3. We fit the phonon lifetimes, and get $c_{3ph} = 19677.7$ and $c_T = 8567.2$ for τ_{3ph} and τ_T in V_{300}. At 300 K, when considering the effects of volumetric expansion together with the temperature-induced renormalization for the phonon and phonon-phonon interaction, due to four-phonon scattering, the phonon lifetime drops by 56%, which is less than that in TDEP-V0
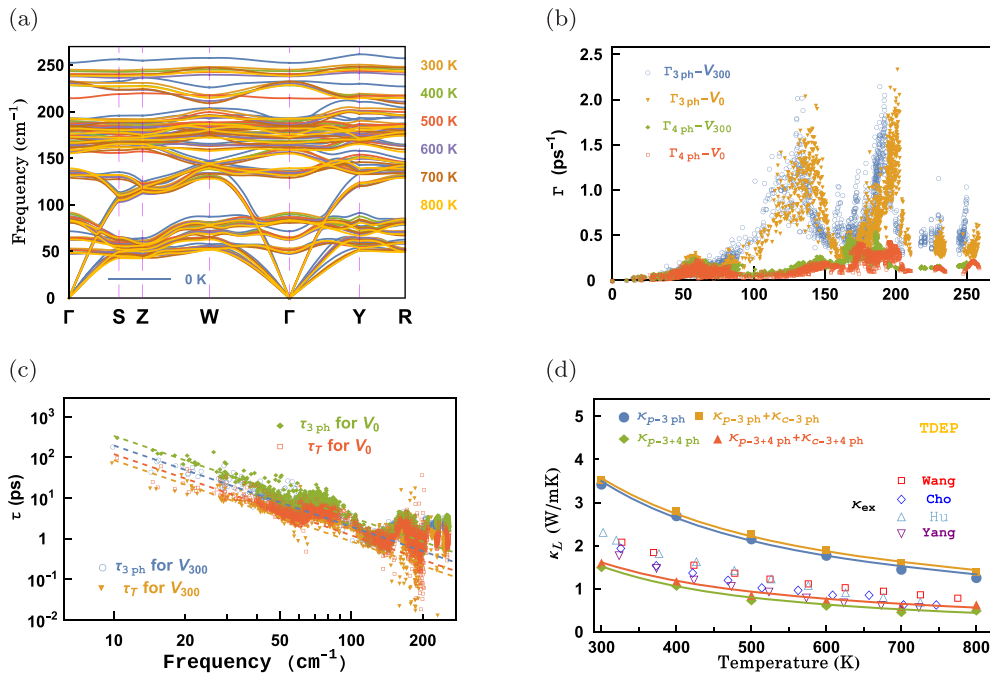

FIG. 12. The effects of volumetric expansion on phonon transport. (a) Phonon spectra (b) three-phonon and four-phonon scattering rate at 300 K, (c) phonon lifetimes at 300 K, and (d) average lattice thermal conductivities with respect to temperature in Cu_2GeSe_3.

TABLE II. Theoretically determined Raman frequencies (in cm^{-1}) and their symmetry assignments of the experimental results [33].

Raman scattering		V_0		TDEP-V_0	TDEP-V_T
Symmetry	Frequency	Symmetry	Frequency	Frequency	Frequency
A_1 or B_1	135	B_1	136.0	137.8	135.7
		A_1	136.7	140.0	134.3
A_2	189	A_2	192.8	196.3	185.3
B_2	212	B_2	191.3	199.1	191.4
A_1 or B_1	235	A_1	232.4	227.6	232.4
A_1 or B_1	254	B_1	252.3	247.5	245.1

FIG. 13. The percentage of κ_c in κ_T for Cu$_2$GeSe$_3$.

(64%) and ShengBTE-V0 (93%) calculations. Then we can conclude that the higher-order phonon-phonon scattering is remarkable in Cu$_2$GeSe$_3$. On the other hand, the temperature-induced renormalization for the phonon and phonon-phonon interaction greatly alleviates higher order anharmonic phonon-phonon interaction. The volumetric expansion would further reduce the influence of four-order phonon-phonon interaction.

We give the temperature-dependent lattice thermal conductivities in Fig. 12(d) by TDEP method after considering the volumetric expansion. Fitting for the lattice thermal conductivity due to three-phonon and four-phonon scattering (merely three-phonon interaction), we get the $b = 1.261$ (0.983). When considering the effect of wavelike interbranch tunneling, the $b = 1.070$ (0.930).

F. Discussion

Next we give some further notes for the phonon transport in Cu$_2$GeSe$_3$ according to present calculations. As shown in Table II, the temperature-induced renormalization for phonon increases the frequencies for the modes with strong four-order phonon-phonon scattering, while it still failed to correct the B_2 modes. After considering the expanse of volume, the frequency of phonon would decrease mostly. Nevertheless, the prediction for the phonon spectrum is relatively satisfactory compared to the experiment.

From the calculation of thermal conductivity, ultimately, the calculation considering higher-order phonon scattering and adding temperature-induced renormalization for the phonon and phonon-phonon interaction, and volumetric expansion effects results into a lower thermal conductivity, while the results considering only higher-order phonon scattering and temperature-induced renormalization effects are in better agreement with the experimental results of thermal conductivities and the behavior of temperature-dependent thermal conductivity for Cu$_2$GeSe$_3$. This may be due to the overestimation of the volume by the PBE method. In Cu$_2$GeSe$_3$, due to the strong four-phonon scattering, the effect of wavelike interbranch tunneling are somewhat strong. For example, when considering the temperature-induced renormalization for phonon and phonon-phonon scattering, the ratio of κ_c/κ_T would be from 5% at 300 K to 27% at 800 K as shown in Fig. 13.

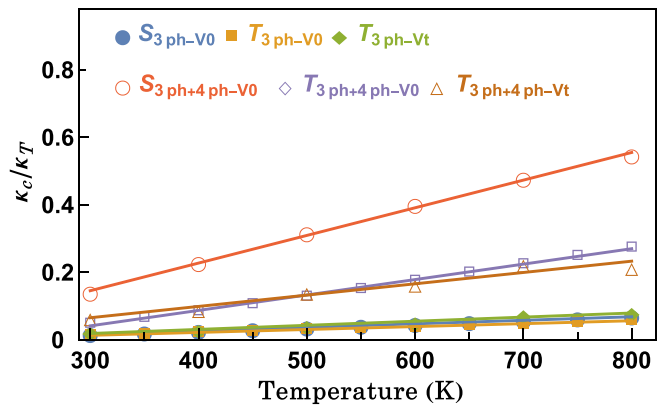We propose here how to determine the strength of four-phonon scattering for Cu$_2$GeSe$_3$ from the temperature-dependent Raman experiments. Generally the spreading of the vibrational peak is proportional to the phonon scattering of phonon mode [52]. Our calculations show that among the various Raman modes of Cu$_2$GeSe$_3$, the A$_2$ mode has the strongest scattering with temperature. And the broadening of linewidth of the Raman peak corresponds to the scattering processes. Our calculations show that the scattering is linearly enhanced with the increasing temperature, when only considering the three-phonon scattering. At low temperature, the scattering rate of the A$_2$ mode is determined by the three-phonon scattering, whereas the four-phonon scattering is gradually enhanced with the increase of temperature. And then the scattering of A$_2$ mode will significantly deviate from the linear behavior of that by three-phonon scattering after the superposition of both. Therefore, we could predict that the broadening of linewidth of the A$_2$ mode will be similar to the above behavior in experiment. Then monitoring such mode in the experiment could be used to estimate the strength of higher-order phonon scattering in Cu$_2$GeSe$_3$, and to further help elucidate the other effects on the phonon transport in Cu$_2$GeSe$_3$.

IV. CONCLUSION

In summary, we have employed first-principles calculations to study the effects of spin-orbit coupling, higher-order phonon-phonon scattering, wavelike coherent propagation, temperature-induced renormalization for the phonon and phonon-phonon interaction, and volumetric expansion on the phonon transport of Cu$_2$GeSe$_3$. Our calculations reproduce well the phonon frequencies of Raman data, except the B$_2$ mode with frequency of 212 cm^{-1}. We further introduce LO-TO splitting and resolve such discrepancy. Though spin-orbit coupling induced slightly increase in the averaged Grüneisen parameters, the scattering rate of low-frequency modes is weakened. Therefore spin-orbit coupling enhances slightly the lattice thermal conductivity of Cu$_2$GeSe$_3$. When only considering three-phonon scattering, the calculated lattice thermal conductivities are much higher than the experimental values, and the predicted behavior of temperature-dependent phonon transport have a large deviation from experiments, which is speculated by the effects of higher-order phonon-phonon interaction. Whereas one adds only

four-phonon scattering for the 0 K equilibrium volume of Cu_2GeSe_3, the amharmonicity would be greatly overestimated and lead to a much lower calculated lattice thermal conductivities than the experimental values. We further find that the temperature-induced renormalization for the phonon and phonon-phonon interaction for the 0 K equilibrium volume of Cu_2GeSe_3 could greatly alleviate the four-phonon scattering while maintaining the three-phonon scattering, and result in consistent lattice thermal conductivities with the experimental values. Furthermore, we study the effects of volumetric expansion and wavelike tunneling of interbranch modes on the phonon transport in Cu_2GeSe_3. Our calculations indicates that the origin of low thermal conductivity of Cu_2GeSe_3 is largely attributed to the four-phonon scattering, which is influenced greatly by temperature-induced renormalization effects. The present work provides a full physical picture for the phonon properties in such Cu-based diamondlike materials and may help design better thermoelectric materials.

[1] *CRC Handbook of Thermoelectrics*, edited by D. M. Rowe (CRC Press, Boca Raton, FL, 1995).

[2] M. Liu, F. Huang, L. Chen, and I. W. Chen, Appl. Phys. Lett. **94**, 202103 (2009).

[3] M. Liu, I. W. Chen, F. Huang, and L. Chen, Adv. Mater. **21**, 3808 (2009).

[4] J. Paier, R. Asahi, A. Nagoya, and G. Kresse, Phys. Rev. B **79**, 115126 (2009).

[5] J. Y. Cho, X. Shi, J. R. Salvador, J. Yang, and H. Wang, J. Appl. Phys. **108**, 073713 (2010).

[6] X. Shi, L. Xi, J. Fan, W. Zhang, and L. Chen, Chem. Mater. **22**, 6029 (2010).

[7] J. Y. Cho, X. Shi, J. R. Salvador, G. P. Meisner, J. Yang, H. Wang, A. A. Wereszczak, X. Zhou, and C. Uher, Phys. Rev. B **84**, 085207 (2011).

[8] Y. Zhang, X. Yuan, X. Sun, B.-C. Shih, P. Zhang, and W. Zhang, Phys. Rev. B **84**, 075127 (2011).

[9] L. Xi, Y. B. Zhang, X. Y. Shi, J. Yang, X. Shi, L. D. Chen, W. Zhang, J. Yang, and D. J. Singh, Phys. Rev. B **86**, 155201 (2012).

[10] H. Shao, X. Tan, T. Hu, G.-Q. Liu, J. Jiang, and H. Jiang, Europhys. Lett. **109**, 47004 (2015).

[11] H. Shao, X. Tan, J. Jiang, and H. Jiang, Europhys. Lett. **113**, 26001 (2016).

[12] H. Shao, H. Zhang, B. Peng, X. Tan, G.-Q. Liu, J. Jiang, and H. Jiang, Europhys. Lett. **115**, 26002 (2016).

[13] R. Wang, A. Li, T. Huang, B. Zhang, K. Peng, H. Yang, X. Lu, X. Zhou, X. Han, and G. Wang, J. Alloys Compd. **769**, 218 (2018).

[14] J. Yang, R. Song, L. Zhao, X. Zhang, S. Hussain, G. Liu, Z. Shi, and G. Qiao, J. Eur. Ceram. Soc. **41**, 3473 (2021).

[15] Z. Hu, H. Xu, C. Yan, Y. Liu, Q. Han, L. Cheng, Z. Li, and J. Song, ACS Appl. Mater. Interfaces **14**, 20972 (2022).

[16] *Thermal Conductivity: Theory, Properties, and Applications*, edited by T. M. Tritt (Kluwer Academic/Plenum Publishers, New York, 2004).

[17] *Topological Insulators*, edited by F. Ortmann, S. Roche, and S. O. Valenzuela (Wiley, New York, 2015).

[18] X.-L. Qi and S.-C. Zhang, Rev. Mod. Phys. **83**, 1057 (2011).

[19] Z. Tian, J. Garg, K. Esfarjani, T. Shiga, J. Shiomi, and G. Chen, Phys. Rev. B **85**, 184303 (2012).

[20] W. Li, L. Lindsay, D. A. Broido, D. A. Stewart, and N. Mingo, Phys. Rev. B **86**, 174307 (2012).

[21] G. Kresse and J. Hafner, Phys. Rev. B **47**, 558 (1993).

[22] G. Kresse and J. Furthmüller, Phys. Rev. B **54**, 11169 (1996).

[23] J. P. Perdew, K. Burke, and M. Ernzerhof, Phys. Rev. Lett. **77**, 3865 (1996).

[24] K. Parlinski, Z. Q. Li, and Y. Kawazoe, Phys. Rev. Lett. **78**, 4063 (1997).

[25] A. Togo, F. Oba, and I. Tanaka, Phys. Rev. B **78**, 134106 (2008).

[26] W. Li, J. Carrete, N. A. Katcho, and N. Mingo, Comput. Phys. Commun. **185**, 1747 (2014).

[27] Z. Han, X. Yang, W. Li, T. Feng, and X. Ruan, Comput. Phys. Commun. **270**, 108179 (2022).

[28] M. Simoncelli, N. Marzari, and F. Mauri, Nat. Phys. **15**, 809 (2019).

[29] See Supplemental Material at http://link.aps.org/supplemental/10.1103/PhysRevB.107.085202 for the atomic position information of Cu_2GeSe_3, the electronic structures, tests of convergence with respect cutoff for fourth-order phonon-phonon interaction and q-point grid, and the detailed implementation of KcMath for calculating the κ_c.

[30] O. Hellman, P. Steneteg, I. A. Abrikosov, and S. I. Simak, Phys. Rev. B **87**, 104111 (2013).

[31] N. Shulumba, O. Hellman, and A. J. Minnich, Phys. Rev. B **95**, 014302 (2017).

[32] E. Parthé and J. Garín, Monatsh. Chem. **102**, 1197 (1971).

[33] G. Marcano, C. Rincón, G. Marín, G. Delgado, A. Mora, J. Herrera-Pérez, J. Mendoza-Alvarez, and P. Rodríguez, Solid State Commun. **146**, 65 (2008).

[34] S. P. Ong, S. Cholia, A. Jain, M. Brafman, D. Gunter, G. Ceder, and K. A. Persson, Comput. Mater. Sci. **97**, 209 (2015).

[35] G. Marcano and L. Nieves, J. Appl. Phys. **87**, 1284 (2000).

[36] B. K. Sarkar, A. S. Verma, and P. Deviprasad, Phys. B: Condens. Matter **406**, 2847 (2011).

[37] H. Shao, X. Tan, G.-Q. Liu, J. Jiang, and H. Jiang, Sci. Rep. **6**, 21035 (2016).

[38] R. M. Pick, M. H. Cohen, and R. M. Martin, Phys. Rev. B **1**, 910 (1970).

[39] Y. Wang, J. J. Wang, W. Y. Wang, Z. G. Mei, S. L. Shang, L. Q. Chen, and Z. K. Liu, J. Phys.: Condens. Matter **22**, 202201 (2010).

[40] Y. Zhang, X. Ke, C. Chen, J. Yang, and P. R. C. Kent, Phys. Rev. B **80**, 024304 (2009).

[41] S. K. Saha, Phys. Rev. B **92**, 041202(R) (2015).

[42] T. Feng, L. Lindsay, and X. Ruan, Phys. Rev. B **96**, 161201(R) (2017).

[43] X. Yang, T. Feng, J. Li, and X. Ruan, Phys. Rev. B **100**, 245203 (2019).

[44] J. M. Ziman, *Electrons and Phonons: The Theory of Transport Phenomena in Solids* (Oxford University Press, Oxford, 1960).

[45] Y. Xia, Appl. Phys. Lett. **113**, 073901 (2018).

[46] X. Yang, J. Tiwari, and T. Feng, Mater. Today Phys. **24**, 100689 (2022).

[47] I. Errea, M. Calandra, and F. Mauri, Phys. Rev. Lett. **111**, 177002 (2013).

[48] I. Errea, M. Calandra, and F. Mauri, Phys. Rev. B **89**, 064302 (2014).

[49] R. Bianco, I. Errea, L. Paulatto, M. Calandra, and F. Mauri, Phys. Rev. B **96**, 014111 (2017).

[50] T. Tadano and S. Tsuneyuki, Phys. Rev. B **92**, 054301 (2015).

[51] D. S. Premkumar, R. Chetty, P. Malar, and R. C. Mallik, AIP Conf. Proc. **1665**, 120020 (2015).

[52] H. Yu, L.-C. Chen, H.-J. Pang, P.-F. Qiu, Q. Peng, and X.-J. Chen, Phys. Rev. B **105**, 245204 (2022).